SINR Maximization Using a STAR-RIS Equipped Large Aperture Antenna for SATCOM Applications

Jafar Norolahi, Tiep M. Hoang, and Alireza Vahid
Department of Electrical and Microelectronic Engineering
Rochester Institute of Technology, Rochester, NY
Emails: {jn3211,tmheme,alireza.vahid}@rit.edu

2025 IEEE 22nd Consumer Communications & Networking Conference (CCNC) | 979-8-3315-0805-0/25/$31.00 ©2025 IEEE | DOI: 10.1109/CCNC54725.2025.10976082

***Abstract*—The rapid increase in the number of satellites increases the amount of signal interference at ground stations, which are typically equipped with large aperture antennas (LAAs). In this work, we propose an interference mitigation solution for satellite communications by placing a simultaneously transmitting and reflecting reconfigurable intelligent surface (STAR-RIS) at the first focal point of the LAA exploiting the existing structure and power supply. The goal is to use the STAR-RIS to improve the signal-to-interference-plus-noise ratio (SINR) of the desired satellite in the presence of multiple interferes. We turn the SINR maximization into fractional programming for which we use Dinkelbach's method to find the STAR-RIS coefficients. Our numerical results reveal the effectiveness of our approach in enhancing the SINR at the ground station.**

***Index Terms*—STAR-RIS, large aperture antennas, SATCOM, interference mitigation, Fractional programming.**

I. Introduction

In satellite communications (SATCOM), Cassegrain antennas play a central role due to their high gain and significant efficiency [1]. However, as the number of signal sources in space increases, so does the amount of interference, which would then be amplified along with the desired signal, degrading signal reception. Further, technologies such as millimeter wave (mmWave) weather radars require large-aperture antennas (LAA) for their measurements [2]. These mmWave radars require antennas with strong polarization isolation, high sidelobe level (SLL), and high gain to achieve more accurate results [3].

The research [4] addresses interference between 5G base stations in the 3.5 GHz range and LLA in satellite earth stations, analyzing scenarios, calculating separation distances, and proposing mitigation strategies like antenna adjustments and power level modifications to ensure coexistence and minimize interference. Additionally, in [5] authors focused on enhancing interference mitigation in radio astronomy through improved antenna pattern modeling for large axisymmetric paraboloidal reflector antennas. They introduced a closed-form expression for the antenna pattern that accounts for focal ratio and feed pattern, and develops adaptive methods to refine this model using real-time interference measurements. By incorporating these advanced models into a modified coherent time-domain canceling (CTC) scheme, the study demonstrates a significant reduction in prediction errors and a slower update requirement for effective CTC, thereby advancing the state-of-the-art in mitigating satellite interference. Using dual-scale modeling, the authors identify damage patterns and deformation mechanisms, providing insights for improving structural durability and protection in space. In [6], the authors analyze interference from small aperture satellite terminals that use a time-division protocol. Due to their larger beamwidths, these terminals can cause significant interference to adjacent satellites. The study quantifies this interference and sets criteria to limit it, considering factors such as antenna pointing errors and rain fading.

Reconfigurable intelligent surfaces (RISs) have attracted a lot of attention in recent years. An RIS is a near-passive device that can manipulate the phase and the amplitude of the incident signal before reflecting it back into the environment. RIS has found applications in communication systems for multiple objectives, such as radio frequency interference cancellation in radio telescopes [7], improving security performance [8], and interference cancellation [9]. Simultaneously transmitting and reflecting reconfigurable intelligent surfaces (STAR-RIS) are attended to. STAR-RIS has superior advantages over traditional RIS, such as providing 360° wireless coverage by enabling signals to pass through the elements' substrate. Unlike conventional RIS, which only reflects wireless signals to users on one side, STAR-RIS offers enhanced performance and flexibility [10]. It has been widely applied to interference cancellation [10], [11].

This work proposes the integration of an STAR-RIS into an LAA to reduce interference in SATCOM systems. To be more specific, we propose to place the STAR-RIS at the first focal point of a parabolic and hypercatabolic reflector of the LAA to reduce the effect of interference and amplify the desired signal received at the feeder as shown in Fig. 1. Placing the STAR-RIS at the first focal point has multiple advantages in interference mitigation and desired signal enhancement, which we will further discuss in Section II. With the STAR-RIS being integrated into the LAA, we carefully optimize the STAR-RIS coefficient and show that the SINR can be significantly improved. Placing the STAR-RIS at the focal point of the LAA is a key enabler of our design and results in effective interference mitigation and improvement of the

This work was in part supported by NSF grants CNS-2343959, CNS-2343964, and AST-2348589. Any opinions, findings, and conclusions are the author(s)' and may not reflect the views of the NSF.

signal-to-interference-plus-noise ratio (SINR).

Notations: $\mathbb{R}$ and $\mathbb{C}$ denote the set of real and complex numbers, respectively. Also, diag$(\cdot)$ denotes a diagonal matrix using the input vector as the diagonal elements; $(\cdot)^T$, $(\cdot)^H$, and $(\cdot)^{-1}$ denote the transpose, Hermitian transpose, and inverse of a matrix, respectively; and $\|\cdot\|$ and $|\cdot|$ denote the ℓ_2 norm and the absolute value of the argument, respectively.

II. System Model

A. Problem Description

In this study, our goal is to improve the SINR at ground stations equipped with a STAR-RIS at the first focal point of LAA. Figure 1 illustrates the geometry of the proposed STAR-RIS-equipped system. The STAR-RIS features a circular antenna array that receives signals and performs beamforming to differentiate between the desired and the undesired signals. Since the sub-reflector should not block the refracting signals, we place all STAR-RIS elements on a disk around the sub-reflector so that STAR-RIS can refract signals without blockage.

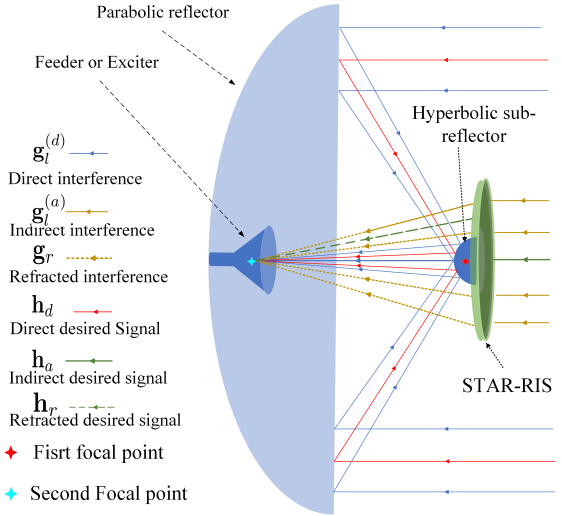

Fig. 1: Illustration of STAR-RIS equipped large aperture antenna.

Figure 2 demonstrates how the proposed system can address SINR in a ground station. As shown, one desired and L undesired satellite signals arrive at the second focal point of an LAA. The role of the STAR-RIS, containing N elements, is to receive the signals coming from space and then refract carefully altered interference and desired signals to the feeder in order to enhance the SINR. The START-RIS adjusts the amplitudes and phases of desired and interference signals on the refracting path to decrease the power of the collected interference signal and increase the power of the desired signal at the feeder. The combination of interference signals from the direct and refracting paths can neutralize each other due to their equal power and opposite phases [7]. Additionally, STAR-RIS helps amplify the desired signal at the feeder when the desired signal from both the refracting and direct paths has the same phase. The amplitudes and phases of the refracted

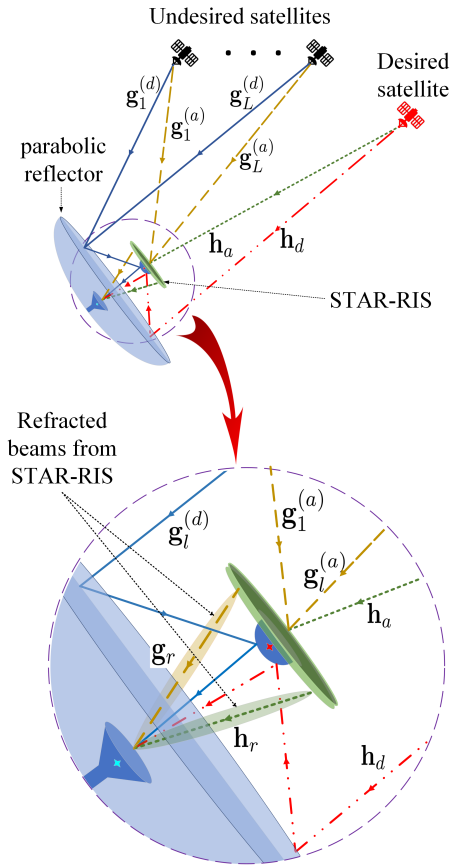

Fig. 2: An illustration of channels from satellites to the feeder of an LAA.

channels are adjusted by STAR-RIS [12]–[14]. Ultimately, the outcome of the STAR-RIS-assisted LAA is an improvement in SINR, achieved through interference suppression and desired signal enhancement.

Remark 1 (Energy Splitting Protocol of STAR-RIS Equipped LAA): Using the Energy Splitting Protocol, all STAR-RIS elements can split the total radiation energy between refraction and reflection modes. Since we assume passive beamforming, the receiving side of the STAR-RIS operates in full passive mode, completely absorbing the signal energy and not reflecting it from its surface pointed toward the sky. Meanwhile, on the refracting side, all N elements of the STAR-RIS operate exclusively in full refraction mode [15], [16].

The primary objective of this paper is to enhance the efficiency of the Large Aperture Antenna, which is often overwhelmed by significant interference, making the reception of the desired signal challenging. Addressing this issue is crucial to ensure effective signal reception. One of the contributions of this paper is the utilization of the first focal point of the LAA for installing the STAR-RIS. This approach offers several advantages, such as leveraging the existing structure that holds

the sub-reflector and power supply, which can also support the STAR-RIS. Additionally, placing the STAR-RIS in the direct boresight of the LAA is beneficial as it would experience the same channels as the LAA experience, enabling effective interference management. Moreover, the typical blockage zone due to the sub-reflector in the first focal point of a Cassegrain antenna can be effectively utilized by the STAR-RIS.

Remark 2 (Impact of LAA beam pattern): It is worth mentioning that installing STAR-RIS at the first focal point may disturb the beam pattern. However, the STAR-RIS would be significantly smaller than a radio telescope and close in size to the sub-reflector, which could minimize the impact on the LAA's beam pattern[1]. In more challenging scenarios, particularly with smaller Cassegrain antennas where the desired signal is completely jammed by unwanted signals, a trade-off can be considered between interference mitigation and the ideal beam pattern or signal reception. In addition, arranging STAR-RIS elements to have better refraction to LAA can be another important issue related to signal propagation in this study. Such cases can be explored in future studies.

B. Signal Model

The proposed system is illustrated in Fig. 2. For one snapshot, denote h_d as the channel from the desired satellite to the LAA through the reflection on the hyperbolic sub-reflector. Denote $\mathbf{h}_a \in \mathbb{C}^{N\times 1}$, $l \in \mathcal{N} \equiv \{1,\ldots,N\}$, as the channel from the desired satellite to the STAR-RIS, and N is the number of elements in STAR-RIS. Denote $\mathbf{h}_r \in \mathbb{C}^{1\times N}$ as the refracting channel from the STAR-RIS to the LAA's feeder. Note that $\mathbf{h}_r$ is associated with the signal from the desired satellite.

Similarly, as for an interfering signal from an undesired satellite l, we will have the following types of channels: i) the channel $\mathbf{g}_l^{(d)} \in \mathbb{C}^{1\times L}$ from the l-th interfering satellite to the feeder through the reflection on the hyperbolic sub-reflector; ii) the channel $\mathbf{g}_l^{(a)} \in \mathbb{C}^{N\times L}$ from the l-th interfering satellite to the STAR-RIS; and iii) the refracting channel $\mathbf{g}_r \in \mathbb{C}^{1\times N}$ from the STAR-RIS to the feeder. Note that $\mathbf{g}_r$ is associated with the signal from the undesired satellites.

Let the transmitted signal from the l-th undesired source be denoted by x_l, with the average transmit power being $E[||x_l||^2] = 1$, and from desired satellites by s. Thus, the received signal at the LAA for one snapshot called $\mathbf{y}$, is given by:

$$\mathbf{y} = \sum_{l\in L}\left(\underbrace{\mathbf{g}_r\text{diag}(\mathbf{v})\text{diag}(\mathbf{w})\mathbf{g}_l^{(a)}x_l}_{\text{indirect undesired}} + \underbrace{\mathbf{g}_l^{(d)}x_l}_{\text{direct undesired}}\right) + \underbrace{\mathbf{h}_r\text{diag}(\mathbf{v})\text{diag}(\mathbf{w})\mathbf{h}_a s}_{\text{indirect desired}} + \underbrace{h_d s}_{\text{direct desired}} + \underbrace{n}_{\text{Noise}}, \quad (1)$$

where $\mathbf{v} \in \mathbb{C}^{N\times 1}$ is defined as the refraction coefficient vector of STAR-RIS that refracts the desired and undesired signals to the feeder. Also, $v_i = |\alpha_i|e^{j\phi_i}$, where $|\alpha_i| \in [0,\alpha_{max}]$, $\alpha_{max} \geq 1$ is the energy coefficient for refracting links and $\phi_i \in [0,2\pi]$. The term n denotes the additive Gaussian noise (AWGN) signal with the mean and power of 0 and σ^2, respectively. Moreover, $\mathbf{w} \in \mathbb{C}^{N\times 1}$ is the receive beamforming vector.

[1]Although, a detailed analysis of the LAA beam pattern is beyond the scope of this work.

C. Assumptions

In this study, we make the following assumptions:

1) LAA and STAR-RIS boresights are aligned.
2) The space blocked by the back of the STAR-RIS does not affect the signals received by the LAA.
3) The LAA is well-constructed and the focal points are correctly positioned. Therefore, the signals reflected off and back to the parabolic reflector and sub-reflector, $\mathbf{h}_d$ and $\mathbf{g}_l^{(d)}$, do not interfere with the STAR-RIS.
4) We assume the channel coefficients are known perfectly.

III. SINR Maximization

In this section, an SINR maximization problem at the feeder is formulated, which occurs when the received desired signals through direct and indirect links are combined at the feeder. Moreover, in this problem, the SINR can be improved by reducing interference at the feeder [12]. From (1), the SINR can be given by

$$\text{SINR} = \frac{\mathcal{U}(\mathbf{w},\mathbf{v})}{\mathcal{V}(\mathbf{w},\mathbf{v})}, \quad (2)$$

where the numerator $\mathcal{U}(\mathbf{w},\mathbf{v})$ and the denominator $\mathcal{V}(\mathbf{w},\mathbf{v})$ are expressed as follows:

$$\mathcal{U}(\mathbf{w},\mathbf{v}) = \left|\mathbf{h}_r\text{diag}(\mathbf{v})\text{diag}(\mathbf{w})\mathbf{h}_a + h_d\right|^2, \quad (3)$$

and

$$\mathcal{V}(\mathbf{w},\mathbf{v}) = \left|\sum_{l\in L}\left(\mathbf{g}_l^{(d)} + \mathbf{g}_r\text{diag}(\mathbf{v})\text{diag}(\mathbf{w})\mathbf{g}_l^{(a)}\right)\right|^2 + |\sigma|^2. \quad (4)$$

In (3), $\left|\mathbf{h}_r\text{diag}(\mathbf{v})\text{diag}(\mathbf{w})\mathbf{h}_a + h_d\right|^2$ represents the power of the retrieved desired signals through direct and indirect channels. Additionally, in (4), $\left|\mathbf{g}_l^{(d)} + \mathbf{g}_r\text{diag}(\mathbf{v})\text{diag}(\mathbf{w})\mathbf{g}_l^{(a)}\right|^2$ describes the power of the interference signals through direct and indirect channels. $|\sigma|^2$ denotes the noise power.

To maximize the SINR at the feeder, the following optimization problem is formulated:

$$\max_{\mathbf{w},\mathbf{v}} \quad \text{SINR} \quad (5a)$$

$$\text{s.t.} \quad \mathcal{V}(\mathbf{w},\mathbf{v}) \leq \epsilon, \quad (5b)$$

$$||\mathbf{w}|| \leq 1, \quad (5c)$$

$$||\mathbf{v}|| \leq \rho, \quad (5d)$$

where the optimization variables $\mathbf{w}$ and $\mathbf{v}$ are designed to maximize the SINR, while ϵ is a threshold that ensures the remaining interference signals at the feeder do not exceed a

predetermined value. ϵ can be experimentally adjusted based on practical conditions. Also, the norm of $\mathbf{w}$ should not exceed 1 to ensure that the signal power is properly scaled and does not artificially amplify noise and interference. Moreover, ρ represents the STAR RIS power budget, which ensures the amplification of refracted signals. Some applications, such as radio astronomy, impose stringent interference power limits captured as constraint (5b) in (5). In other applications, this constraint could be omitted. The problem (5) is a fractional programming (FP) problem, as delineated in [17]. To handle (5), Dinkelbach's method is employed.

A. Fractional Programming Transform

In this part, Dinkelbach's method is used to solve equation (5) iteratively. The process begins by reformulating the fractional objective through Dinkelbach's transform. Subsequently, the problem is recast into an explicit form of $\mathbf{w}$ and $\mathbf{v}$. To achieve this, the introduction of a new auxiliary variable β facilitates the expression of the transformed objective of equation (5) as:

$$\max_{\mathbf{w},\mathbf{V}} \quad \mathcal{U}(\mathbf{w},\mathbf{v}) - \beta\mathcal{V}(\mathbf{w},\mathbf{v}), \tag{6a}$$

$$\text{s.t.} \quad (5b), (5c), (5d), \tag{6b}$$

where β is defined as $\beta = \frac{\mathcal{U}(\mathbf{w},\mathbf{v})}{\mathcal{V}(\mathbf{w},\mathbf{v})}$. Our FP problem, which includes two optimization variables $\mathbf{w}$ and $\mathbf{v}$, should be adapted to a single ratio FP. To achieve this, multiple outer iterations, including several inner iterations, are designed by solving equation (6). This implies that during our algorithm's numerous outer and inner iterations, Dinkelbach's method generates a procedure for each iteration to optimize $\mathbf{w}$, and $\mathbf{v}$. This process is described below and summarized in Algorithm 1.

Algorithm 1 : STAR-RIS Equipped LAA

1: Initialize values for $\mathbf{w}^{[0]}$, $\mathbf{v}^{[0]}$, ϵ
2: **for** $0 \leq t \leq \mathbf{T_{outer}} - 1$ *do*
3: **for** $0 \leq q \leq \mathbf{Q_{inner}} - 1$ *do*
4: Optimize $\mathbf{w}$ using (7)
5: Update $\mathbf{w} \leftarrow \mathbf{w}^*$
6: Update β as: $\beta_{t+1} = \frac{\mathcal{U}(\mathbf{w}^*,\mathbf{v}^{[0]})}{\mathcal{V}(\mathbf{w}^*,\mathbf{v}^{[0]})}$
7: **End for**
8: **for** $0 \leq q \leq \mathbf{Q_{inner}} - 1$ *do*
9: Optimize $\mathbf{v}$ using (8)
10: Update $\mathbf{v} \leftarrow \mathbf{v}^*$
11: Update β as: $\beta_{t+1} = \frac{\mathcal{U}(\mathbf{w}^*,\mathbf{v}^*)}{\mathcal{V}(\mathbf{w}^*,\mathbf{v}^*)}$
12: **End for**
13: Update $\mathbf{w}^{[0]} \leftarrow \mathbf{w}^*$ and $\mathbf{v}^{[0]} \leftarrow \mathbf{v}^*$
14: **End for**
15: **Return** $(\mathbf{w}_{\text{opt}}, \mathbf{v}_{\text{opt}}) = (\mathbf{w}^*_{\text{T}_{\text{outer}}-1}, \mathbf{v}^*_{\text{T}_{\text{outer}}-1})$ as the optimal solution

Firstly, in the inner iteration, it is assumed that $\mathbf{v} = \mathbf{v}^{[0]}$ is constant. The algorithm can be updated at the current $[t+1]$ iterations to optimize $\mathbf{w}$. Thus, (6) would be reformulated by substituting these assumptions.

$$\max_{\mathbf{w}_1} \quad \mathcal{U}(\mathbf{w},\mathbf{v}^{[0]}) - \beta\mathcal{V}(\mathbf{w},\mathbf{v}^{[0]}), \tag{7a}$$

$$\text{s.t.} \quad \mathcal{V}(\mathbf{w},\mathbf{v}^{[0]}) \leq \epsilon, (5c), (5d), \tag{7b}$$

where β is iteratively updated by $\beta_{t+1} = \frac{\mathcal{U}(\mathbf{w}^{[t]},\mathbf{v}^{[0]})}{\mathcal{V}(\mathbf{w}^{[t]},\mathbf{v}^{[0]})}$, t is the iteration index, and $\mathbf{w}^{[t]}$ is the solution obtained by (7). We denote the extracted optimal value of w[t] in the first of the inner iterations part to $\mathbf{w}^*$. The next part of inner iterations with the assumption $\mathbf{w} = \mathbf{w}^*$, will optimize $\mathbf{v}$ by updating (7). The optimal solution of the next part of the inner iterations will be $\mathbf{v} = \mathbf{v}^*$. Therefore, the problem (7) can be updated as follows.

$$\max_{\mathbf{w}^*} \quad \mathcal{U}(\mathbf{w}^*,\mathbf{v}) - \beta\mathcal{V}(\mathbf{w}^*,\mathbf{v}), \tag{8a}$$

$$\text{s.t.} \quad \mathcal{V}(\mathbf{w}^*,\mathbf{v}) \leq \epsilon, (5c), (5d). \tag{8b}$$

As a result of the inner iteration, the obtained optimal solution can be updated as $(\mathbf{w},\mathbf{v}) = (\mathbf{w}^*,\mathbf{v}^*)$ which will be the initial values for the next outer iteration. The next outer and inner iterations are conducted until they converge to the global optimum solution of (6).

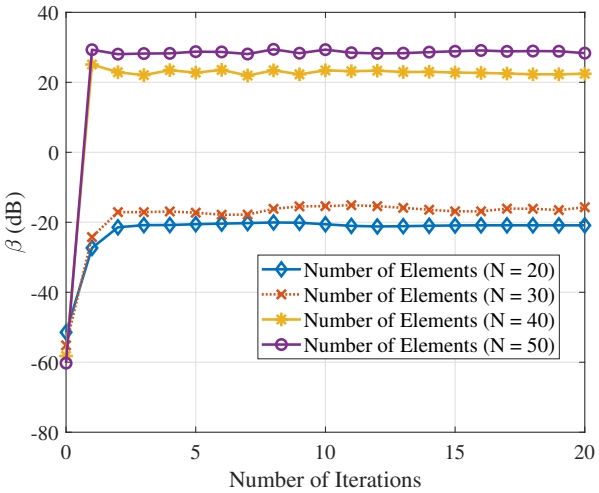

Fig. 3: The convergence pattern of algorithm 1 for different numbers of elements in the STAR-RIS and 40 interfering satellites.

IV. NUMERICAL RESULTS

In Fig. 3, we display the convergence of Algorithm 1 through outer iterations for different numbers of STAR-RIS elements, considering 8 undesired satellites as sources of interference that the algorithm must handle. Stability in this study means that the SINR reaches a consistent level in our curve, indicating that the algorithm can manage a certain level of interference while amplifying the desired signal. This stability depends on conditions such as the power budget for the STAR-RIS, the number of elements, and the number of interference signals. These factors can cause variations in the achieved stable SINR level. In this figure, we plot β versus the number of iterations, where β in each iteration represents the

ratio of desired signal power to interference and noise power. The behavior of β serves as an indicator of the optimization process and SINR trends, not the SINR values.

Our scheme achieves a more stable solution as the number of elements increases. This stability is attributed to the ability of STAR-RIS elements to handle higher interference levels, positively impacting the consistency of the response. In a STAR-RIS, we can define the degree of freedom (DoF), which means that an arrangement of N elements can provide sufficient degrees of freedom to manage up to $N-1$ interference signals [12]. Therefore, in the curves for 20 and 30 elements, the number of interfering satellites (40) is greater than the DoF ($N-1=40-1=39$), where N is the number of elements). In contrast, for the curves with 40 and 50 elements, the DoF exceeds the number of interfering satellites, allowing for better interference management. As a result, we observe a significant gap between the SINR values in these cases. SINR improvements based on the number of elements are evaluated separately in this study, and the results are discussed in Fig. 4. The increasing and stable behavior of β demonstrates the effective performance of the optimization process in Algorithm 1.

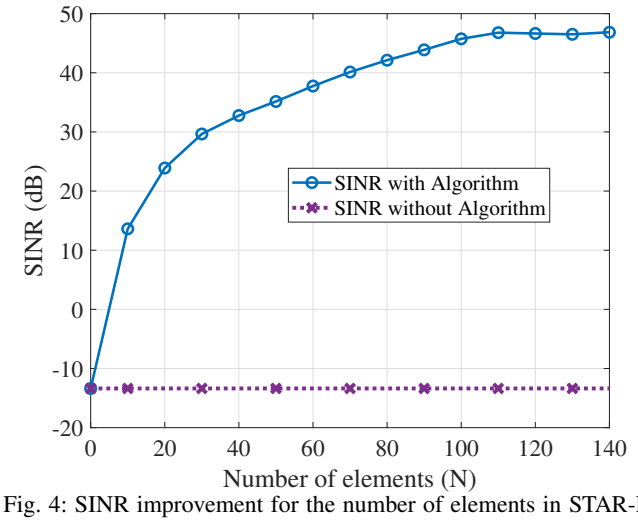

Fig. 4: SINR improvement for the number of elements in STAR-RIS for 8 interfering satellites. LAA without STAR-RIS has an SINR of about -13 dB.

The simulation results of the optimization problem reveal a significant improvement in SINR with the increasing number of elements in STAR-RIS. Fig. 4 shows the SINR results at the feeder of LAA. In this simulation, the number of interfering satellites is 8, and LAA without STAR-RIS has an SINR of -13 dB. As the number of elements in STAR-RIS grows, the SINR experiences a notable enhancement. This improvement can be attributed to STAR-RIS's increased capability to effectively mitigate interference and amplify desired signals, thereby optimizing signal reception at the LAA's feeder. With more elements in STAR-RIS, interference reduction becomes more precise, and the amplification of desired signals becomes more efficient. However, beyond 45 dB, the SINR tends to stabilize, indicating that a certain number of elements for STAR-RIS can effectively eliminate interference. These findings underscore the critical role of STAR-RIS in optimizing satellite communication systems and offer insights into the scalability and effectiveness of the proposed approach in real-world scenarios. Consequently, STAR-RIS enhances the SINR, leading to more efficient data transmission.

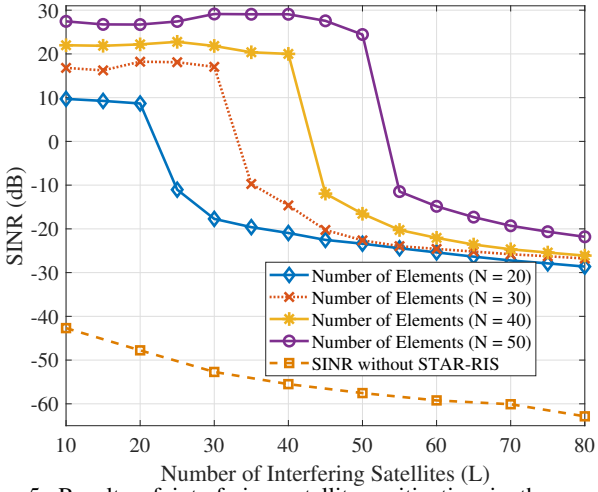

Fig. 5: Results of interfering satellites mitigation in the proposed system.

Additionally, Fig. 5 illustrates multiple evaluations of SINR in the proposed system as the number of interfering signals increases. The bottommost curve represents the SINR of ambient signals, indicating the SINR at the LAA feeder without processing by our algorithm. In this case, the SINR shows a decreasing trend as the number of interfering satellites increases. The remaining curves depict the results of our algorithm's implementation to maximize SINR for varying numbers of elements in the STAR-RIS. The extent of interference suppression directly depends on the number of elements in the STAR-RIS, with more elements allowing for the mitigation of a greater number of interference signals. For $L < N$, the SINR changes gradually, but a noticeable decline occurs when $L \geq N$, showing that when the number of interference signals meets or exceeds the number of STAR-RIS elements, additional undesired signals can overwhelm the LAA. This outcome occurs because an arrangement of N elements provides sufficient DoF to manage up to $N-1$ interference signals [12]. According to the results in this figure, the algorithm can improve SINR and stabilize it before reaching the DoF limit. Beyond this point, as the number of interfering satellites exceeds the DoF, the curves drop but still show a significant improvement in SINR compared to the ambient SINR. Moreover, the SINR improves with an increase in the number of elements, highlighting the STAR-RIS's effectiveness in mitigating interference. Thus, the DoF of the STAR-RIS is crucial for determining the maximum manageable interference count. For example, with $N=30$, the SINR sharply declines once $L \geq 30$, and this pattern is

consistent across other cases. Therefore, Fig. 5 demonstrates that the STAR-RIS offers a substantial advantage in mitigating interference for LAA.

V. Conclusion

This study underscores the potential of STAR-RIS integration in large aperture antennas (LAAs) to enhance satellite communications. We proposed to place a STAR-RIS at the LAA's first focal point, and then used this structure to mitigate undesired interference, and amplify the desired signal, thus, optimizing the SINR. The proposed system, using receive beamforming, demonstrates significant improvements in signal reception at the LAA's feeder, promising enhanced reliability for satellite communication networks. The numerical analysis validates the effectiveness of this approach in reducing interference power, affirming its potential to enhance signal recovery in challenging environments. Leveraging Dinkelbach's transform technique for fractional programming facilitates system performance optimization. The results show that the inclusion of the STAR-RIS noticeably improves the SINR and has a remarkable effect on interference suppression. This work offers insights into STAR-RIS's impact on satellite communication systems. Future studies may delve into fine-tuning system parameters and real-world implementations to further validate its efficacy. Exploring scalability and robustness in diverse conditions could deepen understanding and broaden practical applications.

References

[1] S. Y. Miao and F. H. Lin, "High-gain dual-polarized dual-beam planar 1-bit cassegrain antenna," in *2023 IEEE 11th Asia-Pacific Conf. on Anten. and Prop. (APCAP)*, vol. 1, 2023, pp. 1–2.

[2] J. Wang, H. Lin, F. Yang, G. Xu, and J. Ge, "Design of 94GHz dual-polarization antenna fed by diagonal horn for cloud radars," *IEEE Access*, vol. 10, pp. 22 480–22 486, 2022.

[3] R. R. Neely III and *et al.*, "The NCAS mobile dual-polarisation Doppler X-band weather radar (NXPol)," *Atmospheric Measurement Techniques*, vol. 11, no. 12, pp. 6481–6494, 2018.

[4] L. Liu and B. Wang, "Interference mitigation technology solution for 5G base stations to satellite earth stations," in *2023 International Wireless Communications and Mobile Computing (IWCMC)*, 2023, pp. 700–704.

[5] R. Sengupta and S. W. Ellingson, "Adaptive antenna pattern modeling for interference mitigation in radio astronomy," in *2023 IEEE Conference on Antenna Measurements and Applications (CAMA)*, 2023, pp. 483–488.

[6] V. Weerackody, "Interference analysis for a network of time-multiplexed small aperture satellite terminals," *IEEE Trans. on Aerospace and Electronic Systems*, vol. 49, no. 3, pp. 1950–1967, 2013.

[7] Z. Zou, X. Wei, D. Saha, A. Dutta, and G. Hellbourg, "SCISRS: Signal cancellation using intelligent surfaces for radio astronomy services," in *GLOBECOM 2022 - 2022 IEEE Global Communications Conference*, 2022, pp. 4238–4243.

[8] T. M. Hoang, C. Xu, A. Vahid, H. D. Tuan, T. Q. Duong, and L. Hanzo, "Secrecy-rate optimization of double RIS-aided space–ground networks," *IEEE Internet of Things Journal*, vol. 10, no. 15, pp. 13 221–13 234, 2023.

[9] J. Wu, W. Cheng, J. Wang, J. Wang, and W. Zhang, "RIS-based self-interference cancellation for full-duplex broadband transmission," *IEEE Transactions on Wireless Communications*, vol. 23, no. 7, pp. 7159–7171, 2024.

[10] M. Ahmed and *et al.*, "A survey on STAR-RIS: Use cases, recent advances, and future research challenges," *IEEE Internet of Things Journal*, vol. 10, no. 16, pp. 14 689–14 711, 2023.

[11] T. Hou, J. Wang, Y. Liu, X. Sun, A. Li, and B. Ai, "A joint design for STAR-RIS enhanced NOMA-comp networks: A simultaneous-signal-enhancement-and-cancellation-based (ssecb) design," *IEEE Transactions on Vehicular Technology*, vol. 71, no. 1, pp. 1043–1048, 2022.

[12] Z. Zhang, H. Cao, J. Fan, J. Peng, and S. Liu, "Active RIS-assisted sup-degree of freedom interference suppression for a large antenna array: A deep-learning approach with location awareness," *IEEE Trans. on Anten. and Prop.*, vol. 72, no. 1, pp. 628–641, 2024.

[13] M. Alizadeh, X. Mootoo, O. Waqar, and H. Tabassum, "Qos-aware deep unsupervised learning for STAR-RIS assisted networks: A novel differentiable projection framework," *IEEE Commun. Letters*, pp. 1–1, 2024.

[14] C. Zhou, B. Lyu, S. Gong, and C. You, "Active STAR-RIS-assisted symbiotic radio communications under hardware impairments," *IEEE Commun. Letters*, vol. 27, no. 10, pp. 2797–2801, 2023.

[15] B. Zhao, C. Zhang, W. Yi, and Y. Liu, "Ergodic rate analysis of STAR-RIS aided NOMA systems," *IEEE Commun. Letters*, vol. 26, no. 10, pp. 2297–2301, 2022.

[16] C. Zhang, W. Yi, Y. Liu, Z. Ding, and L. Song, "Star-ios aided NOMA networks: Channel model approximation and performance analysis," *IEEE Trans. on Commun.*, vol. 21, no. 9, pp. 6861–6876, 2022.

[17] K. Shen and W. Yu, "Fractional programming for communication systems—part I: Power control and beamforming," *IEEE Trans. on Sig. Proc.*, vol. 66, no. 10, pp. 2616–2630, 2018.